Available online at www.eccomasproceedia.org
Eccomas Proceedia COMPDYN (2025) 1472-1481

ECCOMAS
Proceedia

COMPDYN 2025
10th ECCOMAS Thematic Conference on
Computational Methods in Structural Dynamics and Earthquake Engineering
M. Papadrakakis, M. Fragiadakis (eds.)
Rhodes Island, Greece, 15-18 June 2025

MACHINE LEARNING BASED FRAMEWORK FOR PREDICTING PRESTRESSING FORCE REDUCTION IN PRESTRESSED REINFORCED CONCRETE BRIDGES

Mirko Calò*[1], Sergio Ruggieri[1], Manuel Buitrago[2], Andrea Nettis[1], Jose M. Adam[2], Giuseppina Uva[1]

[1] DICATECH Department, Polytechnic University of Bari, via E. Orabona 4, 70125, Bari, Italy
e-mail: {mirko.calo, sergio.ruggieri, andrea.nettis, giuseepina.uva}@poliba.it

[2] ICITECH, Universitat Politècnica de València, Camino de Vera s/n, 46022 Valencia, Spain
{mabuimo1, joadmar}@upv.es

Abstract

The paper presents a framework to predict the prestressing force reduction in prestressed reinforced concrete (PSC) bridges via machine learning (ML) algorithms. In the field of structural health monitoring (SHM) of bridges, some difficulties arise in the assessment of specific bridge typologies, such as PSC box-girder bridges. In fact, the challenges posed by the inaccessibility of internal unbonded tendons and the complexity of measuring the effective prestressing force reduction over time do not allow to design an efficient SHM system. Hence, the proposed approach aims to develop a nonlinear modelling strategy, validated on experimental tests on a scaled PSC box-girder, for generating a sample data at the base of the ML model. For training different ML regression models, the variability of several parameters (i.e., geometrical and mechanical properties) was accounted for to ensure generalizability. Results were evaluated by means of statistical metrics and an eXplainability approach. The outcome of the proposed surrogate model consists of simulating the prestressing force reduction based on the knowledge of few parameters, and the use of the eXplainability approach provided the best strategy for designing a sensor-based SHM system.

Keywords: Existing Bridges, Bridge Assessment, Structural monitoring, Box-Girder Bridges, Machine Learning, Prestressing Force.

ISSN:2623-3347 © 2025 The Authors. Published by Eccomas Proceedia.
Peer-review under responsibility of the organizing committee of COMPDYN 2025.
doi: 10.7712/120125.12503.25204

1 INTRODUCTION

Bridges are key assets along transportation networks and safety evaluations are primary concern for road and railway management companies and public institutions to avoid casualties and economic losses. Existing bridge portfolios managed by companies are usually highly populated, and the main challenge, as highlighted by Adam et al. [1], consists of identifying the assets characterized by poor structural conditions and planning future actions (e.g., demolition/reconstruction, retrofit interventions or traffic limitations) after performing structure-specific analysis [2]. The multi-level approach proposed by the Italian government in 2020 [2] was designed encompassing different bridges typologies across the national bridge stock such as prestressed reinforced concrete (PSC) ones. As highlighted by the data analysis performed by Fabre Consortium [3], this construction technology is widely spread over the Italian bridge stock (67% over a sample of 400 bridges) comprehending not only T or double-T girder beams, but also box-girders.

PSC box-girder bridges were designed and built to take advantage of high torsional stiffness, reduced deck height, and higher span length. Nevertheless, some issues characterize the structural assessment of this bridge typology: (i) special inspections are required inside the box for the prestressing system [4], (ii) the prestressing force reduces over time [5]. Regarding this latter, several studies employing different structural health monitoring (SHM) approaches [6-12] pointed out difficulties in the assessment of effective prestressing force value on existing bridges due to materials time-dependent phenomena [13, 14], environmental parameters, and the interaction among degradation processes. Promising SHM strategies involve the use of in-strand fiber Bragg gratings (FBG) [10] and concrete strain sensors [11] although there are some limitations. In-strand FBG cannot be used for existing bridges due to their installation in the construction phase, while concrete strain sensors are effective in the case of linear strain distribution and where a perfect bond between the prestressing strands and surrounding concrete is ensured [12]. In addition, the latter can be placed in each desired section and in variable number. Still, PSC box-girder bridges are often characterized by internal unbonded strands, and, in this case, it is not possible to establish a direct correlation between the strain of concrete fibers and strands. However, recent advancements in Machine Learning (ML) are significantly supporting bridge health management through the integration with SHM data. For example, Kim and Park [15] proposed an Artificial Neural Network (ANN) trained on experimental datasets to estimate the tensile stress on a 50-m real-scale PSC girder with embedded elasto-magnetic sensors.

The inaccessibility of internal unbonded tendons and the complexity of measuring the effective prestressing force reduction over time pose challenges for the design of an efficient sensor-based SHM system. On this basis, this paper presents an ML surrogate model to predict the prestressing force reduction in PSC box-girder bridges. The methodology, described in Section 2, comprise the use of prestressing force initial value (F_0) and other mechanical features evaluated at the time of onsite strain-sensors installation (herein indicate as "initial state") to predict the variation of the prestressing force (F_1). The proposed ML surrogate model is selected among three different ML regression algorithms (i.e., ANN, Random Forrest Regressor, RFR and Support Vector Regression, SVR) after their training and test phases over sample data generated with a nonlinear FE modelling approach. Moreover, the physical description of results through an eXplainability approach, named Shapley Additive exPlanation (SHAP) [16] allowed investigating the proper design of a sensors-based SHM system. The effectiveness of the nonlinear FE modelling strategy and of the framework was validated in Section 3 through experimental tests on a scaled beam specimen in the ICITECH laboratories of *Universitat Politècnica de València*. ANN was identified as the best ML surrogate model for this task, and the SHAP approach was used to determine the key parameters influencing F_1. The results provided new insights that could aid in designing optimized sensor-based SHM for critical structural components. The main conclusions of the study are presented in Section 4.

2 ML SURROGATE MODEL FRAMEWORK

The proposed ML surrogate model, Figure 1, is designed through a model-driven approach that considers physical and mathematical methods to establish an input-output relationship. The input variables considered to predict the output F_1 (from the initial state onwards) are F_0 and the elastic modulus of concrete (E_c) at the time of onsite strain-sensors installation, and the values of strain variations ($\Delta\varepsilon^{(i,j)}$) measured at different fibers of different sections of the girder, (superscript $^{(j)}$ and $^{(i)}$ respectively). Interested readers can find more information about the framework in [17].

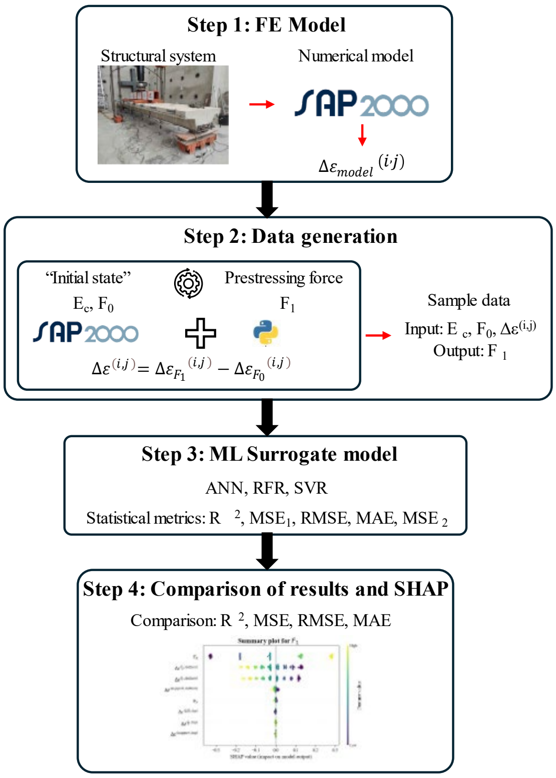

Figure 1: Workflow of the proposed ML surrogate model.

The first step of the proposed framework involves the definition of a nonlinear finite element (FE) model of the PSC box-girder bridge once geometry (dimensions of the sections, position of the steel rebars and tendons in each section), F_0, material properties, and boundary conditions are known. The proposed FE modelling strategy, validated towards experimental results as later shown (Section 3), includes frame elements and a diffuse plasticity approach with fibers. Although representing a balance between accuracy of numerical results and simplicity of the simulation, this strategy allows reducing the number of parameters used as input variables in the ML surrogate model and facilitating data generation for ML model training. Regarding the typology of plasticity to be implemented in the FE model, a deformation-controlled PMM plasticity is selected, which allows considering the external axial load due to prestressing (P) and the bi-directional bending in both main section axes (MM) induced by the prestressing force and the external loads. On this basis, fixed an external load (e.g., four-point test of the experimental campaign in Section 3), the strain increment under a generic prestressing force value, $\Delta\varepsilon_{F_k}{}^{(i,j)}$, can be computed.

The second step regards data generation for training and testing ML algorithms. Assuming a statistical distribution (e.g., uniform) for uncertain input parameters as F_0 and E_c, strain increments $\Delta\varepsilon^{(i,j)}$, given a fixed value of E_c, can be computed as:

$$\Delta\varepsilon^{(i,j)} = \Delta\varepsilon_{F_1}{}^{(i,j)} - \Delta\varepsilon_{F_0}{}^{(i,j)} \tag{1}$$

where F_0 is the prestressing force at the "initial state" and F_1 is its final value, representing the prestressing force reduction. The quantification of E_c and F_0 require both destructive and non-destructive tests, and the maximum reduction rate of F_0 (i.e., F_1) should be calibrated case-by-case.

The dataset generated in the second step is required to train ML algorithms candidate as ML surrogate model. In this study, the ML algorithms selected are ANN, RFR, and SVR. ANN was selected for its capacity to generalise problems, despite the necessity of tuning a substantial number of hyperparameters. RFR was chosen for its resilience against overfitting and its simple hyperparameter tuning. SVR, representing a compromise between the two previous algorithms, exhibits both robustness against overfitting and challenges in hyperparameter tuning. Each ML algorithm is trained and tested splitting the database in 80/20 and the predictive accuracy can be assessed through the definition of some statistical metrics: coefficient of determination (R^2), Mean Squared Error (MSE_1), Root Mean Squared Error (RMSE), Mean Signed Error (MSE_2) and Mean Absolute Error (MAE). In this case, the chosen statistical metric for selecting the ML surrogate model is the MSE_2, because in this application it is important to distinguish between positive and negative errors. Since a smaller value of F_1 is conservative and thus reflects a positive value of error by the ML model, ML surrogate model characterized by positive MSE_2 in both training and test phase is preferred. On the other hand, the RMSE is the best way to compare the accuracy of ML models, because it is in the same unit as the output itself.

In the end, to improve understanding of black-box models as the ML surrogate model, eXplainability metrics such as SHAP can provide insights into predictions. SHAP evaluates the influence of features based on all the features in the dataset using combinatorial calculus. The importance of each feature is determined by its average SHAP value and its relationship with the target variable.

3 RESULTS OF THE APPLICATION TO A SCALED PSC BOX BRIDGE

In this section the results of the application to a scaled PSC box bridges are presented and discussed. The framework described in Section 2 was applied following the steps summarized in Figure 2.

The considered specimen was a scaled PSC box-girder bridge tested in the ICITECH laboratory of the *Universitat Politècnica de València*. The specimen (Figure 3) is a 6 m box-girder supported by hinged and hinged-roller supports. Geometrically, both beam ends are solid for a length of 0.40 m, while the end part in the middle is lightened by expanded polystyrene (i.e., hollow section, Figure 3). The prestressing system is characterized by three steel bars with 20 mm of diameter (B500C), housing in three polyvinyl chloride tubes and anchored through bolts with steel plates interposed to the end faces of the beam after stringing operations. The final value of prestressing force F_0 applied to the specimen was to 330 kN, which resulted in 110 kN of stringing force and a stress equal to 350 MPa on each bar. The specimen was equipped by: (i) ten linear variable displacement transducers (LVDTs) to measure the vertical displacements, (ii) twenty-one embedded strain gauges to monitor concrete deformations, three at both ends of

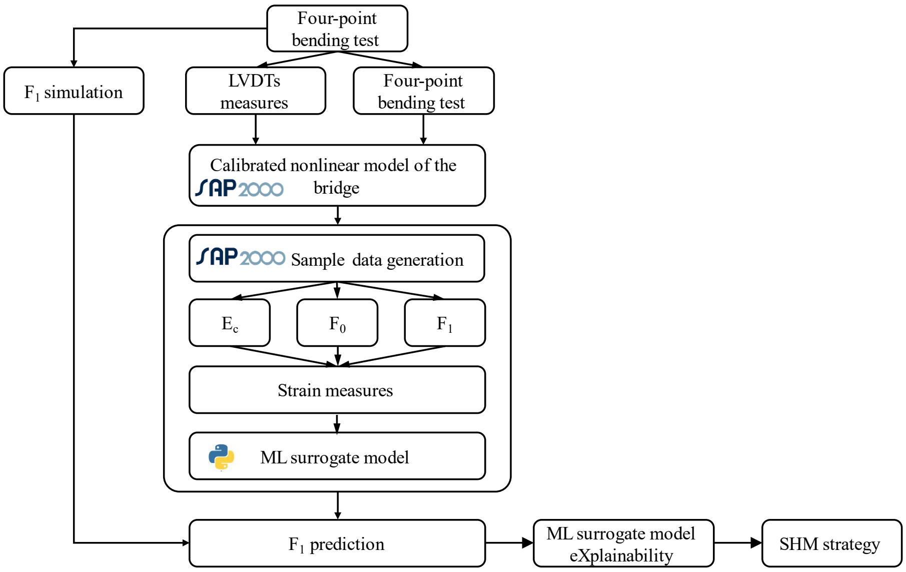

Figure 2 - Framework application on an experimental case.

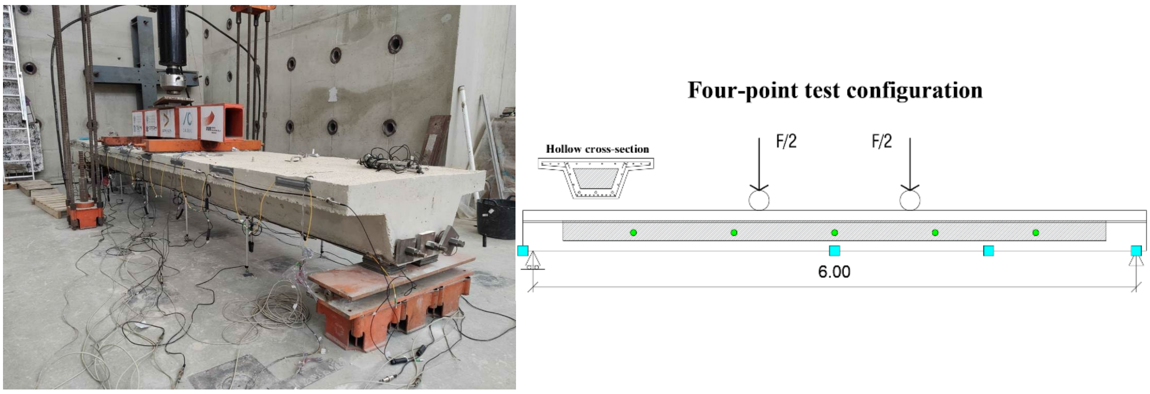

Figure 3 – PSC box-girder under loading protocol of Phase 1 “undamaged” (green dots represent distribution of LVDTs, while cyan squares the box-beam sections monitored through strain-sensors).

Compressive strength [MPa]	Tensile strength [MPa]	Elastic modulus E_c [MPa]
34.99	2.35	39464
31.34	3.01	36741
32.12	2.93	32412

Table 1: Results of mechanical tests on concrete cylinders after 45 days.

the prestressing steel bars (i.e., six sensors) and five at bottom part of middle span, quarter span and hinged support sections (i.e., fifteen sensors). In addition, FBG sensors were placed for the entire length of the bridge, in the same vertical position of strain sensors and in the upper face to provide strain increments on top fibers. Mechanical properties of concrete, summarized in Table 1, were evaluated before the experimental campaign through cylindrical specimens at 45 days after casting.

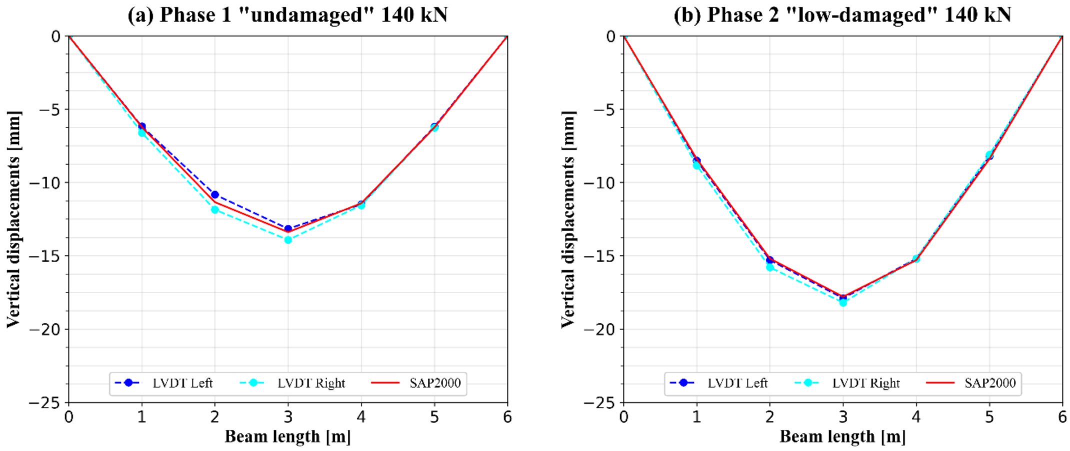

Figure 4 – Comparison between numerical (a) and experimental (b) vertical displacement values for 140 kN steps on Phase 1 "undamaged". All the values are expressed in millimeters; therefore, all vertical deformed shapes are on a 1000:1 scale with respect to beam length.

The experimental program was designed to assess the impact of prestressing loss on box beam deformations. The laboratory tests were divided into four different phases named progressively from Phase 1 "undamaged" to Phase 4 "high-damaged" (the other two, Phas2 and Phase 3, are named "low-damaged" and "moderate-damaged", respectively). During Phase 1, the beam was tested in its initial state, that is with F_0 equal to 330 kN. At the end of each phase, steel bars were removed one at a time until Phase 4 in which the specimen was no longer prestressed. At each stage, the external load was applied through a Four-point bending test (Figure 3) and the values of vertical displacements and $\Delta\varepsilon^{(i,j)}$ were recorded. Different loading values were reached: (i) 140 kN at the end of the first three phases (i.e., 1, 2, and 3), and (ii) 210 kN to failure in Phase 4. The loading protocol in the first three phases of the test was designed to ensure quasi-elastic behavior of the specimen. Furthermore, to avoid a significant effect of one test on the subsequent one, the damage was incremental, and specimen did not exhibit cracks.

LVDTs measurements were used to calibrate the numerical output of the FE model of the specimen simulated through the SAP2000 structural software [18]. According to the modelling strategy introduced in Section 2, plastic hinges were placed at the same sections monitored by strain-gauges and those sections were divided into X direction and Y direction for a total of235 and 207 fibers, for solid and hollow-section respectively. The results of the "trial-and-error" calibration (Figure 4) by changing only the E_c (final value of E_c equal to 38150 MPa) justifies the use of this simplified nonlinear numerical model for the next steps. Indeed, the negligible difference of numerical and experimental vertical displacements in Phase 1 ("undamaged") and Phase 2 ("low-damaged"), is on average by 1.2% and 0.7%, respectively, for a load step of 140 kN (Figure 4). The obtained value of E_c is in good agreement with the average of the three concrete cylindric specimens after 45 days, which is 36200 MPa, with a 5% difference.

Given the calibrated nonlinear numerical FE model, 5000 numerical models were generated by varying E_c between 30 and 40 GPa and simulating progressive prestressing losses F_1 through the reduction of the tendons area for many values of F_0. For each numerical model, input (F_0, E_c, $\Delta\varepsilon^{(i,j)}$) and output ($F_1$) parameters of the ML algorithms were stored and later the dataset was split into training and test data. The values of statistical metrics described in Section 2, obtained after hyperparameter tuning of ML algorithms, are reported in Table 2 for both training and test set. The optimal values obtained from each ML model justify the choice about the candidates as ML surrogate model. Nevertheless, ANN is the only ML surrogate model to meet the requirements about MSE_2 (0.00061/0.00064) outperforming SVR and RFR when considering RMSE (ANN: 0.0019/0.0021, RFR: 0.0938/0.03301, SVR: 0.0255/0.0257).

Set	Metric	ANN	RFR	SVR
Training	R^2	0.9999	0.9999	0.9945
	MAE	0.0016	0.0058	0.0216
	MSE_1	4.12E-06	0.0088	6.5E-04
	RMSE	0.0019	0.0938	0.0255
	MSE_2	6.13E-04	1.53E-03	-1.42E-03
Test	R^2	0.9999	0.9999	0.9845
	MAE	0.0017	0.0229	0.0213
	MSE_1	4.57E-06	0.1090	6.5E-04
	RMSE	0.0021	0.3301	0.0257
	MSE_2	6.44E-04	-4.58E-03	-1.00E-03

Table 1: Results of mechanical tests on concrete cylinders after 45 days.

ML Surrogate model	F_1 calculated [kN]	F_1 experimental [kN]	Difference [%]
ANN	219.43	220	0.3%
RFR	219.13	220	0.4%
SVR	209.78	220	4.6%

Table 2: ML surrogate models F_1 calculated values on Phase 2 "low-damaged" measurements.

After defining the three ML models, their predictive capacity (Table 2) was assessed against the experimental tests that occurred in Phase 2, "low-damaged", which was characterized by the removal of one bar over three, with a F_0 equal to 330 kN and a F_1 equal to 220 kN. Once again, the ML surrogate model made by ANN confirmed the best accuracy, having a percentage difference in terms of F_1 of 0.3%.

Finally, the SHAP eXplainability approach was applied to the proposed ML surrogate model to assess the influence of each considered input (i.e., F_0, E_c, $\Delta\varepsilon^{(i,j)}$) parameter on the simulated prestressing loss, F_1. Figure 5 reports the summary plot and some of the dependence plots. The summary plot ranks input features in ordinate on the base of their influence on the results, and reports in abscissa the value of the impact of each feature on the predictive capacity of the model. The yellow colour of the dots indicates an increasing output value for the observed input value of the feature, while the violet colour denotes the decreasing of the output value. As expected, the most influential input feature is F_0. The second and the third influent parameters are the strain measures at the bottom fiber of the $L/2$ section, $\Delta\varepsilon^{(L/2,\ bottom)}$, and bottom fiber of $L/4$ section, $\Delta\varepsilon^{(L/4,\ bottom)}$. The colour of dots changes from yellow to violet when F_0 increases, from which it can be deduced that F_1 increases as F_0 increases. On the contrary, an increment in $\Delta\varepsilon^{(L/2,\ bottom)}$ and $\Delta\varepsilon^{(L/4,\ bottom)}$ corresponds to an F_1 decrease. Further conclusions can be drawn by looking at the dependence plots of the variables, where a positive trend in the graphs (e.g., F_0) implies that as the input value increases, the output value, F_1, increases and vice versa. Moreover, in the dependence plots, the input variable that may have an interaction effect with the plotted feature is represented in the colormap. For F_0 values above 0.5, a reduction in $\Delta\varepsilon^{(L/4,\ bottom)}$ increases the SHAP value of F_0, while for F_0 values below 0.5, an increase in $\Delta\varepsilon^{(L/4,\ bottom)}$ value decreases the SHAP value of F_0. Conversely, for input feature values $\Delta\varepsilon^{(L/2,\ bottom)}$ and $\Delta\varepsilon^{(L/4,\ bottom)}$ above 0.5, a decrement in E_c reduces the SHAP value of the input feature. For the same features, while their values are below 0.5, an increment in E_c increases the SHAP value.

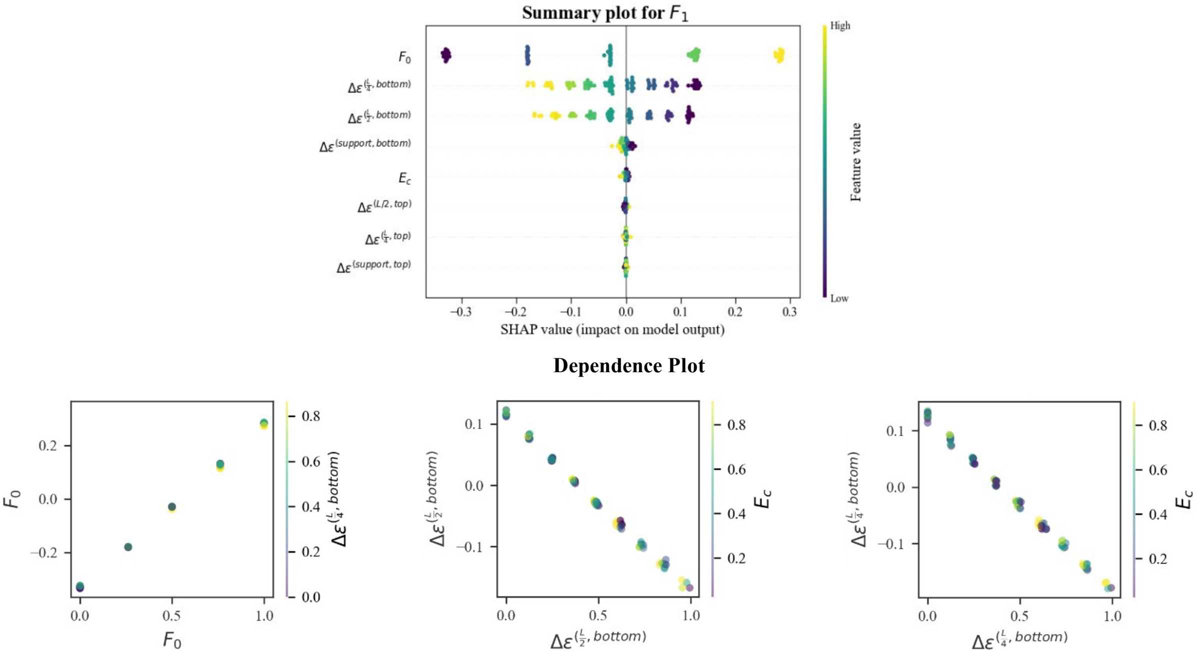

Figure 5 – SHAP summary plot and dependence plot for F_1 output feature.

The mathematical relationship proposed by the ANN is easy to capture, as higher values of E_c correspond to smaller strain increments, and therefore a lower prestressing force reduction.

4 CONCLUSIONS

The paper presented a framework to predict the prestressing force reduction in prestressed rein-forced concrete (PSC) bridges via Machine Learning (ML)-based surrogate model. The goal was to monitor the effective prestressing force reduction over time, and the design of an effective structural health monitoring (SHM) system. To these scopes, the proposed framework is based on the results obtained by experimental tests on a scaled PSC box-girder bridge, made in the ICITECH laboratory of the *Universitat Politècnica de València*. The instrumented scaled box-girder specimen was tested under a Four-point bending test on different phases, from un-damaged (i.e., Phase 1) to progressively damaged (i.e., Phases 2, 3, 4) and from the experi-mental recorded values, a simple but effective nonlinear Finite Element (FE) model was developed and validated. The defined modelling approach, accounting for the variability for geometrical and mechanical properties (i.e., the elastic modulus of concrete (E_c) and prestress-ing force at the "initial state", F_0), was used to populate a sample dataset by defining 5000 FE models. These data were used to train and test three ML algorithms (Artificial Neural Network, ANN, Random Forrest Regressor, and Support Vector Regression) to establish a relation be-tween the prestressing losses (i.e., F_1) and the input variables (i.e., E_c, F_0, and the strain varia-tion in different sections, $\Delta\varepsilon^{(i,j)}$). Using appropriate evaluation metrics, the prediction provided by ANN was the most accurate, revealing the best algorithm to define the ML surrogate model. In addition, the ML surrogate model was investigated through an eXplainability approach achieving the following results: (i) a proper definition of F_0 is required in the "initial state", (ii) the value of E_c presents a low impact on the overall results, even though its role is fundamental in the definition of $\Delta\varepsilon^{(i,j}$, and (iii) an effective sensors-based SHM system for this typology of bridge and for this specific application, can be achieved by placing strain gauges at the bottom fibers of L/2 and L/4 sections (L is the length of the beam).

5 ACKNOWLEDGMENTS

The work of the first and last author was partially funded by the innovation grant "HAMMON" (hazard mapping and vulnerability monitoring) and by the research project PNRR M4C2, Spoke 5, High Performance Computing, Big Data and Quantum Computing," code CN_00000013, CUP: D93C22000430001. The work of the first author was partially funded by Italian Ministry of University and Research, within the project 'PON-Ricerca e Innovazione-2014–2020, CUP Code (D.M. 10/08/2021, n. 1061): D95F21002340006. Sergio Ruggieri acknowledges funding by Italian Ministry of University and Research, within the project 'PON-Ricerca e Innovazione-2014–2020, CUP Code (D.M. 10/08/2021, n. 1062): D95F21002140006. Manuel Buitrago declares funding received under the postdoctoral Grant IJC2020-042642-I funded by MCIN/AEI/ 10.13039/501100011033 and by the "European Union NextGenerationEU/PRTR". Andrea Nettis and Giuseppina Uva acknowledge the Sustainable Mobility National Research Center (MOST) and received funding from the European Union Next-GenerationEU (PIANO NAZIONALE DI RIPRESA E RESILIENZA (PNRR) – MISSIONE 4 COMPONENTE 2, INVESTIMENTO 1.4 – D.D. 1033 17/06/2022, CN00000023) - SPOKE 7 "CCAM, Connected Networks and Smart Infrastructure" - WP4 (CUP D93C22000410001). Finally, Jose M. Adam and all co-authors acknowledge the invaluable cooperation of the Calsens Spin-off company during the execution of the test of the scaled bridge.

6 REFERENCES

[1] J.M. Adam, N. Makoond, B. Riveiro, M. Buitrago. Risks of bridge collapses are real and set to rise — here's why. Nature. 2024, 629, 1001–1003. https://doi.org/10.1038/d41586-024-01522-6.

[2] Ministero delle Infrastrutture e dei Trasporti. "Linee Guida per la Classificazione e Gestione del Rischio, la Valutazione della Sicurezza ed il Monitoraggio dei Ponti Esistenti", Italy, 2020.

[3] W. Salvatore, G. Uva, I. Venanzi, et al. Application of Italian Guidelines for structural-foundational and seismic risk classification of bridges: the Fabre experience on a large bridge inventory. *Proceedings of II Fabre Conference – Existing bridges, viaducts and tunnels: research, innovation and applications*, 2024. https://doi.org/10.1016/j.prostr.2024.09.009

[4] J. Corven. Post-Tensioned Box Girder Design Manual. Federal Highway Administration. (2015). https://www.fhwa.dot.gov/bridge/concrete/hif15016.pdf

[5] M. Yang, J. Gang, X. Yang. Refined calculation of time-dependent prestress losses in prestressed concrete girders. *Structure Infrastructure Engineering* (2020), 16(10), 1430-1446. https://doi.org/10.1080/15732479.2020.1712438

[6] A. Dall'Asta, L. Dezi. Discussion on "Prestress force effect on vibration frequency of concrete bridges" by Saiidi M. et al., *Journal of Structural Engineering* (1996), 122(4). https://doi.org/10.1061/(ASCE)0733-9445(1996)122:4(459)

[7] A. Dall'Asta, G. Leoni. Vibrations of beams prestressed by internal frictionless cables. *Journal of Sound and Vibration* (1999), 222(1), 1-18. https://doi.org/10.1006/jsvi.1998.2066

[8] G. Park, H. Sohn, C.R. Farrar, D. J. Inman. Overview of piezoelectric impedance-based health monitoring and path forward. *Shock and Vibration Digest*. (2023), 35(6), 451-463. https://doi.org/10.1177/05831024030356001

[9] D. Rabelo, R.M. Finzi Neto, V. Steffen. Impedance-Based Structural Health Monitoring incorporating compensation of temperature variation effects. *23rd ABCM International Congress of Mechanical Engineering*, RJ, Brazil. (2015). https://doi.org/10.20906/CPS/COB-2015-1903

[10] S-Z. Cheng, G. Wu, T. Xing, D-C. Feng. Prestressing force monitoring method for a box girder through distributed long-gauge FBG sensors. *Smart Material and Structures* (2018), 27. https://doi.org/10.1088/1361-665X/aa9bbe

[11] C. Liu, J. Teng, N. Wu. A wireless strain sensor network for structural health monitoring. *Shock and Vibration* (2015). https://doi.org/10.1155/2015/740471

[12] H. Abdel-Jaber. Comprehensive strain-based methods for monitoring prestressed concrete beam-like elements. *Ph.D. Thesis: Princeton University*. (2017).

[13] H. Huang, S-S. Huang, K. Pilakoutas. Modeling for Assessment of Long-Term Behavior of Prestressed Concrete Box-Girder Bridges. *Journal of Bridge Engineering* (2018), 23(3). https://doi.org/10.1061/(ASCE)BE.1943-5592.0001210

[14] B. Tu, Y. Dong, Z. Fang. Time-dependent reliability and redundancy of corroded prestressed concrete bridges at material, component, and system levels. *Journal of Bridge Engineering* (2019), 24(9). https://doi.org/10.1061/(asce)be.1943-5592.0001461

[15] J. Kim, S. Park. Field applicability of a machine learning–based tensile force estimation for pre-stressed concrete bridges using an embedded elasto-magnetic sensor. *Structural Health Monitoring* (2020), 19(1), 281-292. https://doi.org/10.1177/1475921719842340

[16] M.L. Scott, S-I. Lee. A Unified Approach to Interpreting Model Predictions. Proceedings of the 31st Annual Conference on Neural Information Processing Systems, Long Beach, CA. (2017). https://doi.org/10.48550/arXiv.1705.07874

[17] M. Calò. S. Ruggieri, M. Buitrago, A. Nettis, J.M. Adam, G. Uva. An ML-based framework for predicting prestressing force reduction in reinforced concrete box-girder bridges with unbonded tendons. *Engineering Structures* (2025), 325, 119400. https://doi.org/10.1016/j.engstruct.2024.119400

[18] Computer and Structures I. SAP2000, Advanced 25. Structural Analysis Program-Manual – Computer and Structures, Inc, Berkeley, California, USA, 2025.